Experimental full-solid-angle substrate photoelectron-diffraction data at 1-keV energies: Implications for photoelectron holography

J. Osterwalder, T. Greber, A. Stuck, and L. Schlapbach
Institut de Physique, Université de Fribourg, CH-1700 Fribourg, Switzerland
(Received 19 August 1991)

Experimental photoelectron distributions of Al 2*s* emission above Al(001) and Pt 4*f* emission above Pt(110) are presented, measured over much of 2π solid angle at high angular resolution. These intensity maps illustrate very clearly the relative importance of various scattering processes. In addition to forward scattering along high-density atomic chains, concentration of photoelectron flux along dense atomic planes is observed. Al 2*s* and Pt 4*f* exhibit very similar intensity patterns associated with equivalent low-index directions. Holographic information about atomic positions within the nearest-neighbor shell around emitter atoms is found to be contained in circular interference fringes in the vicinity of ⟨011⟩ forward-scattering directions.

Angle-scanned photoelectron diffraction (PD) has had its place among the important surface structural techniques for more than a decade.[1,2] Some early experiments had been aimed at obtaining a full picture of the angular distribution of photoelectron intensities over a large part of the hemisphere above a single-crystal sample.[3] Due to the time-consuming data-acquisition procedure, this represents a formidable task, and except for a few studies,[4–6] people contented themselves with just measuring selected line scans in either polar or azimuthal directions. The resulting intensity modulations are by now rather well understood in terms of photoelectron scattering and diffraction, and model calculations carried out at various degrees of sophistication in most cases reach at least a semiquantitative agreement with experiment.[1]

Very recently, the interest in full hemispherical data sets has increased by realizing that such intensity maps could be viewed as photoelectron holograms.[7] In this context, the unscattered photoelectron wave plays the role of the reference wave and the ensemble of all scattered waves that of the object wave. Standard Fourier-transform methods can then be used to obtain three-dimensional real-space images of the near-neighbor shells of the photoemitter, with no more need for cumbersome trial-and-error simulations.[8] Several 2π hemispherical data sets have since been simulated theoretically[8(a),9,10] and some have also been measured experimentally,[11,12] with the result that atomic positions can in many cases be seen, but with limited resolution and with erroneous features appearing at unphysical sites. A straightforward application of such a Fourier-transform approach to an unknown structure seems therefore rather problematic. We here try a more intuitive approach to uncover which features in a full 2π scan carry the holographic information.

To this purpose we present two intensity maps measured over much of 2π solid angle at a rather high angular resolution of approximately 1.0° full cone. The two maps for Al 2*s* emission from Al(001) and Pt 4*f* from Pt(110), both at photoelectron kinetic energies above 1 keV, reveal some characteristic two-dimensional patterns that have not been recognized before with such clarity in substrate PD data. Specifically, bands of enhanced intensity are observed along projections of high-density crystal planes. Moreover, it is found that ⟨001⟩, ⟨011⟩, and ⟨111⟩ crystal axes are associated with three distinct two-dimensional intensity patterns that are very similar for these two differently oriented fcc surfaces.

All experiments have been performed in a Vacuum Generators ESCALAB MarkII spectrometer which is equipped with a two-axis goniometer of a design similar to that described by Fadley.[1(a)] We have developed a data-acquisition system that permits fully automated recording of two-dimensional intensity maps in a tolerable amount of time with a conventional hemispherical electron-energy analyzer and a triple-Channeltron detector. The sample is mounted on the goniometer which has both axes driven by computer-controlled stepping motors. The angle scanning is done in an azimuthal fashion. The polar emission angle is first set to rather grazing ($\theta_{\max}=78°$ off normal) and is then reduced by $\Delta\theta=2°$ after each full azimuthal rotation. The azimuthal step size $\Delta\phi$ is increased as $\Delta\phi=\Delta\theta\theta_{\max}/\theta$ toward lower polar angles θ to give an almost uniform sampling density across the hemisphere. In this way a total of about 3500 angular settings is scanned with an accuracy of the order of 0.2°. At each setting a photoelectron spectrum containing the signal of interest is recorded, and the photoelectron intensity is evaluated in real time by a curve-fitting procedure, which considerably reduces statistical errors as compared to conventional background subtraction procedures.[13]

Oriented and mechanically polished Al(001) and Pt(110) crystals have been cleaned by repeated ion bombardment (Ar, 750 eV) and annealing cycles (Al, 550 °C; Pt, 800 °C). The crystalline order was verified by low-energy electron diffraction, which also showed the Pt(110) surface to be in the 1×2-reconstructed state. Scan times were 23 and 17 h for Al 2*s* and Pt 4*f*, respectively, during which time both surfaces collected less

than half a monolayer of oxygen and carbon contamination at a pressure of 5×10^{-11} mbar.

In Fig. 1(a), the Al 2s intensity map above Al(001) is presented, recorded at a kinetic energy of 1136 eV (Mg $K\alpha$ excitation). The raw data are shown in the stereographical projection, i.e., with radii proportional to $\tan(\theta/2)$, which is conformal and maps circles into circles. Intensities are given in a linear gray scale representation, with no correction for instrumental response. There has been no symmetry averaging, i.e., the almost perfect 4-mm symmetry gives confidence in the high accuracy of this data set.

The intensity scale is dominated by the very strong forward-scattering maxima along ⟨011⟩ nearest-neighbor directions. A second phenomenon, which has not yet been observed with such clarity in photoelectron diffraction data, is the appearance of well-defined sets of bands connecting these forward-scattering maxima. From Fig. 1(b), it is easily seen that these bands are centered at positions of high-density (111) and (001) crystal planes. Along these bands the intensity is still modulated. In addition, there are characteristic features like the Y-shaped intensity enhancements along ⟨111⟩ directions and the eight-leafed flower pattern around [001], which here is the normal direction in the center of the image. Before going into more detail, we compare this intensity map to the one shown in Fig. 2(a), representing the Mg $K\alpha$-excited Pt 4f intensity measured above a Pt(110) surface. Here, the photoelectron kinetic energy is 1184 eV and thus rather similar as in the Al 2s experiment. Although the two data sets of Figs. 1(a) and 2(a) have been obtained from two materials with very different scattering powers—a low-Z nearly-free-electron metal and a high-Z noble metal—and two different surface orientations, a closer inspection of the data brings up surprising similarities. The threefold-symmetric Y-shaped features along ⟨111⟩ directions and the eight-leafed flower patterns around ⟨100⟩ directions are clearly visible in the Pt 4f image, and so are the bands with three of them crossing along ⟨011⟩ directions. Again, these bands correlate rather well with projections of the same high-density crystal planes, and the intensity along these bands is modulated in a way similar to that in the Al 2s case. Even though such similarities have not been recognized before, they may not be too surprising in view of the same crystal structure (fcc) and the fairly similar lattice constants of Al and Pt (4.05 and 3.92 Å, respectively). At these high energies, where forward scattering is strong, subsurface emitters mainly determine the diffraction patterns and give them a rather bulklike character.

The observation of intensity bands along high-density planes appears to be a rather general phenomenon for fcc crystals which we very recently observed also in Cu LVV Auger and Cu 2p (Si $K\alpha$) emission from Cu(001).[14] In

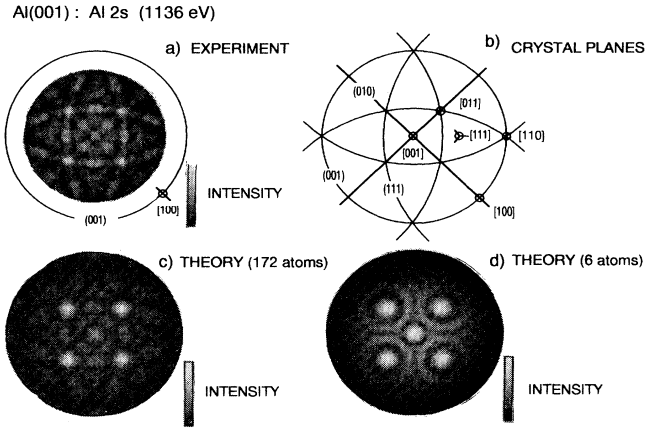

FIG. 1. (a) Experimental Al 2s (Mg $K\alpha$) photoelectron intensity map measured up to polar angles of 78° away from the surface normal of Al(001). Raw data are shown in a linear gray scale representation, with no correction for instrumental response, the intensity scale covering a range from 1400 to 5733 integrated counts. No symmetry operations have been done to the data, which are presented in the stereographic projection. (b) Locations of high-density crystal planes and near-neighbor chains above Al(001). (c) Simulated Al 2s intensity map using a single-scattering formalism and a $3\times3\times3$ unit-cell cluster (see text). (d) Same as (c), but using a small cluster with one Al 2s emitter sitting at the bottom corner of an Al octahedron (see text).

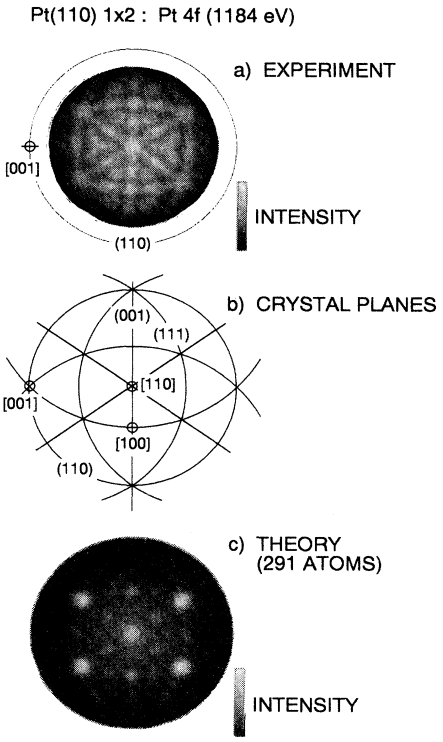

FIG. 2. (a) Experimental Pt 4f photoelectron intensity map above a Pt(110) crystal, using Mg $K\alpha$ radiation for excitation. Here, the intensity scale ranges from 8216 to 43 922 counts. (b) Location of high-density crystal planes and near-neighbor chains above Pt(110). (c) Simulated Pt 4f intensity map using a single-scattering cluster formalism and a $6\times6\times3$ unit-cell cluster (see text).

the very first experimental 2π photoelectron intensity map, a study of Au $4f$ (Al Kα) emission from Au(001) by Baird, Fadley, and Wagner[3] at a kinetic energy of 1403 eV, these bands were not seen as clearly as such (the [001] eight-leafed flower pattern and the $\langle 111 \rangle$ Y pattern, however, can be clearly seen in their data). Still, a qualitative interpretation in terms of Kikuchi bands, i.e., bands of enhanced intensity inside a region of twice the Bragg angle along low-index planes, was used to explain most of the prominent features. Bragg angles of the two densest planes that have nonzero structure factors, (111) and (002),[15] are of the order of only 5°, and these planes indeed correspond to the intensity bands that can be seen in our data. By comparing single-scattering cluster calculations with results from Kikuchi-band theory it had also been concluded that these theories may represent two conceptually different approaches to electron diffraction, one emphasizing the short-range, the other the long-range aspect.[15,16]

From Figs. 1(a) and 2(a) it therefore appears that such substrate photoelectron diffraction images reflect the forward-projected real-space geometry of high-density atomic chains and planes. If there is any holographic information in these patterns, it should not be related to the positions of such bands which do not move with energy. It should therefore be mostly contained in the intensity modulations along the bands or around the chains. In order to study the true diffractive—or holographic—character of the various features, it is useful to compare these images to those obtained by model calculations. Figure 1(c) shows a simulation of the Al $2s$ data, using a single-scattering cluster formalism with spherical-wave scattering of a proper p-wave final state. A fairly small cubic cluster of $3\times3\times3$ unit cells (172 atoms) has been used, with one emitter being placed in the center of each horizontal plane. The details of these calculations are given elsewhere.[1,17] At first sight two qualitative assessments of these calculations can be given: First, all the bands and other characteristic patterns are rather well reproduced, and second, all bands and forward-scattering peaks appear somewhat broadened in the simulated map. This second observation is undoubtedly due to the neglect of multiple scattering (MS) in our calculations. MS effects have been shown to lead to a considerable sharpening of forward-scattering peaks along dense atomic chains,[18,19] and it appears now that a similar phenomenon may be happening with MS within atomic planes.

Similar qualitative effects are seen in the simulated Pt $4f$ intensity map which is shown in Fig. 2(c). Here, a much larger cluster of $6\times6\times3$ unit cells (291 atoms) has been used representing the 1×2 missing-row reconstructed surface with a 15% inward relaxation of the top layer.[20] This calculated image gives the impression of being strongly "overexposed" due to the dramatic overemphasis of forward scattering along nearest-neighbor chains. This effect is much stronger here than in Al due to the stronger attractive ion potential of Pt (see also Ref. 19). However, in addition to the five bright $\langle 011 \rangle$ spots one can faintly recognize the intensity bands and the eight-leafed flower patterns associated with the two $\langle 100 \rangle$ directions.

We now return to the question whether the holographic information can be separated from the purely geometrical features in these 2π intensity maps. It has already been pointed out by Tong *et al.*[10] and by Hardcastle *et al.*[12] that the dominant contribution to holographic interference fringes should be located in the vicinity of forward-scattering maxima. This can actually be seen in the model calculation for Al $2s$ emission shown in Fig. 1(c). Around each of the four $\langle 011 \rangle$ forward-scattering maxima a ring of weaker intensity can be recognized, which, as one moves radially away from $\langle 011 \rangle$, is followed by a ring on which several strong intensity enhancements are located. This is more clearly visible in Fig. 1(d), showing a single-scattering simulation for a six-atom octahedron cluster formed by one emitter in the third layer, four $\langle 011 \rangle$ nearest neighbors above, and one [001] second-nearest neighbor in the top layer, to give the five prominent maxima. Here, the interference fringes can be seen up to third order for $\langle 011 \rangle$ neighbors, but at most to first order for [001]. The ring-shaped intensity depressions between zeroth and first order around $\langle 011 \rangle$ directions can still be seen in the experimental data of Fig. 1(a) in the form of a thinning of the intensity bands in just these regions. The radii of these fringes are not very much affected by MS present in the experiment. It is therefore the angle $\theta_{\langle 011 \rangle}$ between $\langle 011 \rangle$ directions and the first ring of enhanced intensity that carries the holographic information on the bond distance along $\langle 011 \rangle$, primarily through the single-scattering phase relationship $kd_{\langle 011 \rangle}(1-\cos\theta_{\langle 011 \rangle})+\psi(\theta_{\langle 011 \rangle})=2\pi$.[1] By simply measuring $\theta_{\langle 011 \rangle}$ from Fig. 1(a) one finds a value of $25°\pm2°$, which yields [with a magnitude of the **k** vector of $k=17.3$ Å^{-1} and a scattering phase shift of $\psi(\theta_{\langle 011 \rangle})=1.8\pm0.1$ (Ref. 21)] $d_{\langle 011 \rangle}=2.76\pm0.44$ Å for the bond length along $\langle 011 \rangle$. This value is within the error limit associated with photoelectron holography[8(b)] of the true value of 2.86Å.

From this qualitative discussion of 2π intensity maps it appears that first-order interference fringes are seen clearly only for the nearest-neighbor shell around the photoemitter, but also that these are strong enough to dominate over forward-scattering effects involving atoms further away. Even at the fairly high angular resolution used in this study, this is the range over which one may hope to extract atomic positions through forward-scattering photoelectron holography.

A well-polished and oriented Pt(110) crystal has been kindly provided by K. H. Rieder. Skillful technical assistance by F. Bourqui, O. Raetzo, and H. Tschopp has made these experiments possible. This work has been supported by the Schweizerischen Nationalfonds.

[1](a) C. S. Fadley, Prog. Surf. Sci. **16**, 275 (1984); (b) C. S. Fadley, in *Synchrotron Radiation Research: Advances in Surface Science,* edited by R. Z. Bachrach (Plenum, New York, 1989).

[2]W. F. Egelhoff, Jr., Crit. Rev. Solid State Mater. Sci. **16**, 213 (1990).

[3]R. J. Baird, C. S. Fadley, and L. F. Wagner, Phys. Rev. B **15**, 666 (1977).

[4]J. Osterwalder, E. A. Stewart, D. Cyr, C. S. Fadley, J. Mustre de Leon, and J. J. Rehr, Phys. Rev. B **35**, 9859 (1987); E. A. Stewart, M. S. thesis, University of Hawaii, 1987 (unpublished).

[5]H. Li and B. P. Tonner, Phys. Rev. B **37**, 3959 (1988).

[6]M. Seelmann-Eggebert and H. J. Richter, J. Vac. Sci. Technol. B **9**, 1861 (1991).

[7]A. Szöke, in *Short Wavelength Coherent Radiation: Generation and Applications,* edited by D. T. Atwood and J. Boker, AIP Conf. Proc. No. 147 (American Institute of Physics, New York, 1986).

[8](a) J. J. Barton, Phys. Rev. Lett. **61**, 1356 (1988); (b) J. J. Barton, J. Electron Spectrosc. Relat. Phenom. **51**, 37 (1990).

[9]C. M. Wei, T. C. Zhao, and S. Y. Tong, Phys. Rev. Lett. **65**, 2278 (1990).

[10]S. Y. Tong, C. M. Wei, T. C. Zhao, H. Huang, and Hua Li, Phys. Rev. Lett. **66**, 60 (1991).

[11]G. R. Harp, D. K. Saldin, and B. P. Tonner, Phys. Rev. B **42**, 9199 (1990).

[12]S. Hardcastle, Z. L. Han, G. R. Harp, J. Zhang, B. L. Chen, D. K. Saldin, and B. P. Tonner, Surf. Sci. Lett. **245**, L190 (1991).

[13]J. Osterwalder (unpublished).

[14]D. Naumović, A. Stuck, T. Greber, J. Osterwalder, and L. Schlapbach (unpublished); A. Stuck, D. Naumović, H. A. Aebischer, T. Greber, J. Osterwalder, and L. Schlapbach (unpublished).

[15]S. M. Goldberg, R. J. Baird, S. Kono, N. F. T. Hall, and C. S. Fadley, J. Electron Spectrosc. Relat. Phenom. **21**, 1 (1980).

[16]R. Trehan, J. Osterwalder, and C. S. Fadley, J. Electron Spectrosc. Relat. Phenom. **42**, 187 (1987).

[17]D. J. Friedman and C. S. Fadley, J. Electron Spectrosc. Relat. Phenom. **51**, 689 (1990).

[18]M. L. Xu and M. van Hove, Surf. Sci. **207**, 215 (1989).

[19]H. A. Aebischer, T. Greber, J. Osterwalder, A. P. Kaduwela, D. J. Friedman, G. S. Herman, and C. S. Fadley, Surf. Sci. **239**, 261 (1990).

[20]E. Kirsten and K. H. Rieder, Surf. Sci. **222**, L837 (1989).

[21]M. Fink and J. Ingram, At. Data **4**, 129 (1972).

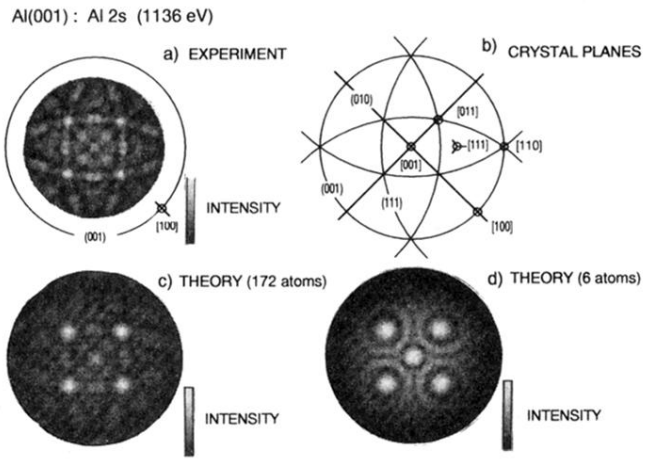

FIG. 1. (a) Experimental Al 2*s* (Mg $K\alpha$) photoelectron intensity map measured up to polar angles of 78° away from the surface normal of Al(001). Raw data are shown in a linear gray scale representation, with no correction for instrumental response, the intensity scale covering a range from 1400 to 5733 integrated counts. No symmetry operations have been done to the data, which are presented in the stereographic projection. (b) Locations of high-density crystal planes and near-neighbor chains above Al(001). (c) Simulated Al 2*s* intensity map using a single-scattering formalism and a $3\times3\times3$ unit-cell cluster (see text). (d) Same as (c), but using a small cluster with one Al 2*s* emitter sitting at the bottom corner of an Al octahedron (see text).

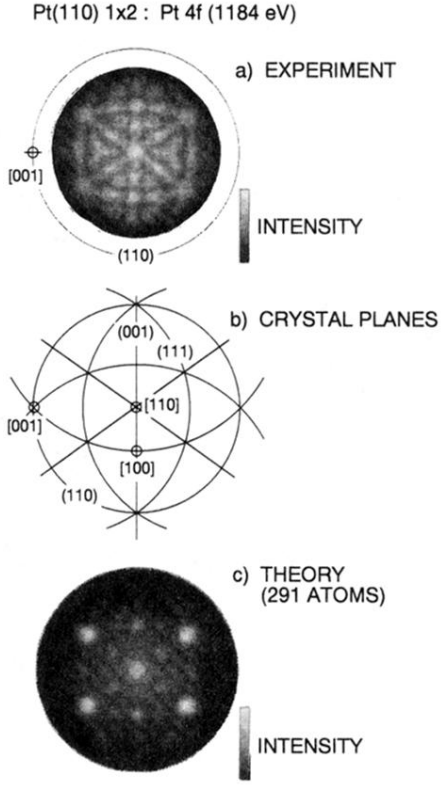

FIG. 2. (a) Experimental Pt $4f$ photoelectron intensity map above a Pt(110) crystal, using Mg $K\alpha$ radiation for excitation. Here, the intensity scale ranges from 8216 to 43 922 counts. (b) Location of high-density crystal planes and near-neighbor chains above Pt(110). (c) Simulated Pt $4f$ intensity map using a single-scattering cluster formalism and a $6\times6\times3$ unit-cell cluster (see text).